nature climate change

SUPPLEMENTARY INFORMATION

DOI: 10.1038/NCLIMATE1816

Spectral biases in tree-ring climate proxies

Jörg Franke

(franke@giub.unibe.ch)

Swiss Federal Research Institute WSL, Birmensdorf, Switzerland,

Institute of Geography, University of Bern, Switzerland and

Oeschger Centre for Climate Change Research, Bern, Switzerland

David Frank

Swiss Federal Research Institute WSL, Birmensdorf, Switzerland and

Oeschger Centre for Climate Change Research, Bern, Switzerland

Christoph C. Raible

Physics Institute, University of Bern, Switzerland and

Oeschger Centre for Climate Change Research, Bern, Switzerland

Jan Esper

Department of Geography, University of Mainz, Germany

Stefan Brönnimann

Institute of Geography, University of Bern, Switzerland and

Oeschger Centre for Climate Change Research, Bern, Switzerland

December 20, 2012

S1 Proxy characteristics

The diversity of proxy-specific characteristics complicates their use in climate reconstructions. Each proxy type or even individual records has particular ways in which climatic signals of interest as well as noise are fingerprinted in the archives. This is a challenge in its own, but also contributes to the need to often employ study specific statistical methods. Proxies can be annually resolved and include high- and low-frequency variability (Fig. S1a, [1]), or capture only either frequency component of variability (Fig. S1b, nc008 from the International Tree Ring DataBase, ITRDB). Values can be continuous or discrete (Fig. S1c, [2]). The temporal resolution can be constant or variable (Fig. S1d, [3]) and the variance can be stationary or changing over time (Fig. S1e, [4]). Proxies can reach thresholds (Fig. S1f, [5]) and thus not record the complete range of climate variability and datasets can also have gaps (Fig. S1g, [6], here filled by linear interpolation between 1100 and 1500 AD).

The records presented in Fig. S1 all pass the correlation screening for annual temperature following the procedure discussed in [7] although not all the records are interpreted as temperature proxies by the authors [5]. Mostly proxies better represent a seasonal rather than an annual mean but nevertheless correlate significantly with yearly averages (e.g. [1]). Thus, proxies are used in reconstructions of annual averages although their seasonality leads to a decrease in signal-to-noise ratio. Note, most proxies in Fig. S1 have been excluded from this study because they do not have annual resolution or do not pass our proxy screening.

S2 Proxy data and screening

Proxy data considered in this study include annually resolved, normalized chronologies that extend back to 1500 AD from the collection by [7]. These records are complemented by additional series that are at least 500 years in length and have annual resolution (Table S1): Norway: [8, pers. comm.], [9]; Sweden: [10], [11], [12]; Central Europe: [13], French Alps: [14]; Swiss Alps: [15], [1], [16]; Greater Alpine Region [17]; Austria: [18], [19], [16]; Italy: [20, updated]; Pyrenees: [21]; Carpathians: [22]; Morocco: [23] Pakistan: [24], [25], [26]; Kirgistan: [27]; China: [28], [29]; Siberia: [30]; Alaska: [31, 32, 33]; Canada: [34], [35] and USA: [36].

We verify the climate sensitivity of the proxy records and to subdivide the proxy dataset into temperature vs. precipitation recording series (see Methods section in main text). From our proxy set no records pass both the screening for temperature and precipitation. The screening results in 56 (128) temperature (precipitation) sensitive proxy records (Tab. S1 and Tab. S2).

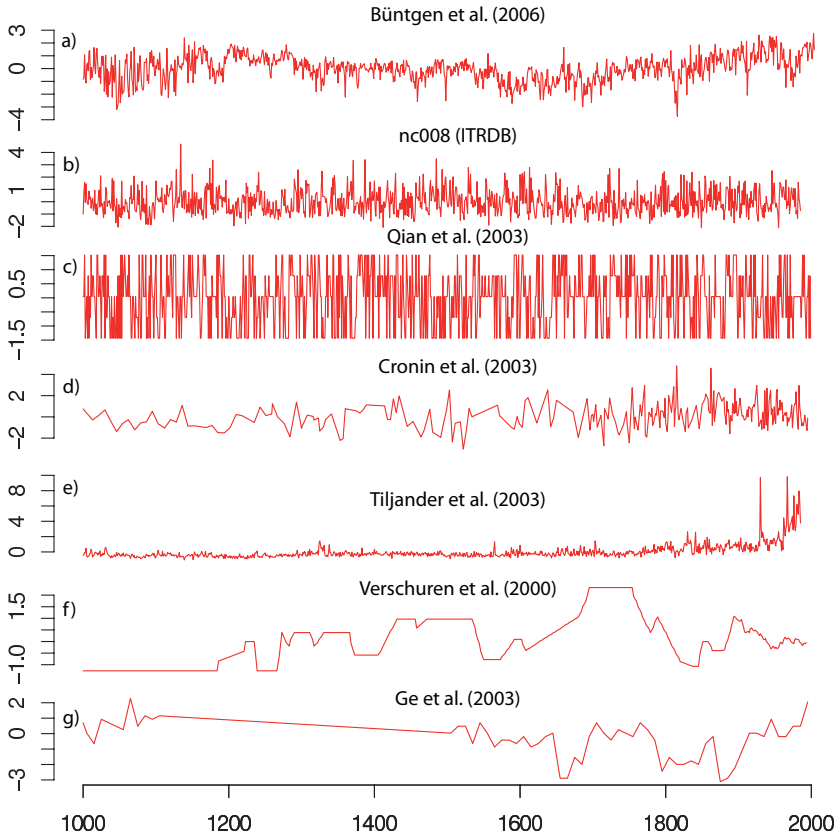

Figure S1: Proxy records covering the last millennium with different characteristics: tree-ring series a) [1] and b) nc008 (Stahle, D.W.; ITRDB), indexed documentary-based records c) and g) [2, 6] and sediment proxies d) e) and f)[3, 4, 5].

Table S1: Proxy records that passed the temperature screening. Correlation coefficient are calculated with respect to the corresponding grid cell in the CRU TS3 dataset [37] for temperature. Effective degrees of freedom are used to take autocorrelation into account.

Code	**r**	**DF**	**DF$_{eff}$**	**Proxy**	**Publication**
ak020	0.24	87	33	TRW	ITRDB
ak021	0.35	91	29	TRW	ITRDB
arge013	0.42	70	22	TRW	ITRDB
arge091	0.26	89	37	TRW	ITRDB
buentgen_2005	0.53	98	13	TRW	Büntgen et al. 2005
buentgen_2006	0.51	100	42	MXD	Büntgen et al. 2006
buentgen_2009	0.43	100	38	TRW	Büntgen et al. 2009
buntgen_science_JJA_temp	0.38	99	24	TRW	Büntgen et al. 2011
ca082	0.34	76	59	TRW	ITRDB
ca529	0.28	83	25	TRW	ITRDB

Table S1: Proxy records that passed the temperature screening. Correlation coefficient are calculated with respect to the corresponding grid cell in the CRU TS3 dataset [37] for temperature. Effective degrees of freedom are used to take autocorrelation into account.

Code	**r**	**DF**	**DF$_{eff}$**	**Proxy**	**Publication**
ca630	0.32	95	63	TRW	ITRDB
ca631	0.25	95	53	TRW	ITRDB
cana110	0.27	88	31	TRW	ITRDB
carpathian	0.21	101	22	TRW	Popa et al. 2008
corona_2009	0.41	96	28	TRW+MXD	Corona et al. 2009
dolomites	0.34	101	24	TRW	Carrer et al. 2007 (updated)
forfjord	0.41	101	101	TRW	Kirchhefer et al. (pers. comm.)
gisp2o18	0.41	83	40	Ice core ^{18}O	Stuiver et al. 1995
grudd	0.41	100	51	MXD	Grudd et al. 2008
jamtland	0.46	102	49	TRW+MXD	Gunnarson et al. 2011
junipars	0.28	96	56	TRW	ITRDB
lapland	0.25	94	77	TRW	Helama et al. 2009
mexi027	0.34	89	38	TRW	ITRDB
mexi027e	0.29	89	66	TRW	ITRDB
mexi027l	0.26	88	37	TRW	ITRDB
mill_pyrenees_MJJAS	0.6	101	91	TRW	ITRDB
nv513	0.23	78	33	TRW	ITRDB
orokonztr	0.51	94	51	TRW	Cook et al. 2002
schweingruber_mxdabd_grid1	0.34	56	66	MXD	Briffa et al. 2002
schweingruber_mxdabd_grid10	0.44	56	75	MXD	Briffa et al. 2002
schweingruber_mxdabd_grid100	0.42	56	60	MXD	Briffa et al. 2002
schweingruber_mxdabd_grid11	0.43	56	49	MXD	Briffa et al. 2002
schweingruber_mxdabd_grid110	0.3	56	79	MXD	Briffa et al. 2002
schweingruber_mxdabd_grid111	0.38	55	66	MXD	Briffa et al. 2002
schweingruber_mxdabd_grid115	0.48	56	36	MXD	Briffa et al. 2002
schweingruber_mxdabd_grid12	0.36	55	33	MXD	Briffa et al. 2002
schweingruber_mxdabd_grid16	0.38	56	44	MXD	Briffa et al. 2002
schweingruber_mxdabd_grid18	0.54	56	45	MXD	Briffa et al. 2002
schweingruber_mxdabd_grid19	0.37	56	45	MXD	Briffa et al. 2002
schweingruber_mxdabd_grid2	0.33	56	58	MXD	Briffa et al. 2002
schweingruber_mxdabd_grid20	0.32	56	74	MXD	Briffa et al. 2002

Table S1: Proxy records that passed the temperature screening. Correlation coefficient are calculated with respect to the corresponding grid cell in the CRU TS3 dataset [37] for temperature. Effective degrees of freedom are used to take autocorrelation into account.

Code	**r**	**DF**	**DF$_{eff}$**	**Proxy**	**Publication**
schweingruber_mxdabd_grid21	0.39	56	77	MXD	Briffa et al. 2002
schweingruber_mxdabd_grid22	0.41	56	88	MXD	Briffa et al. 2002
schweingruber_mxdabd_grid3	0.29	56	60	MXD	Briffa et al. 2002
schweingruber_mxdabd_grid30	0.4	56	28	MXD	Briffa et al. 2002
schweingruber_mxdabd_grid42	0.68	56	53	MXD	Briffa et al. 2002
schweingruber_mxdabd_grid44	0.49	56	40	MXD	Briffa et al. 2002
schweingruber_mxdabd_grid45	0.57	56	52	MXD	Briffa et al. 2002
schweingruber_mxdabd_grid70	0.29	56	53	MXD	Briffa et al. 2002
schweingruber_mxdabd_grid87	0.45	56	45	MXD	Briffa et al. 2002
schweingruber_mxdabd_grid88	0.41	56	62	MXD	Briffa et al. 2002
schweingruber_mxdabd_grid89	0.53	56	33	MXD	Briffa et al. 2002
tyrol_mxd	0.43	93	87	MXD	Esper et al. 2007
vallee_merveille	0.47	102	20	TRW	Büntgen et al. 2012
vinther_2004_scgreenland	0.52	66	45	Ice core ^{18}O	Vinther et al. 2004
wa064	0.38	75	27	TRW	ITRDB
r = Correlation coefficient					
DF = Degrees of Freedom					
DF$_{eff}$ = effective DF taking autocorrelation into account					
TRW = Tree Ring Width					
MXD = Maximum Latewood Density					

Table S2: Proxy records that passed the precipitation screening. Correlation coefficient are calculated with respect to the corresponding grid cell in the CRU TS3 dataset [37] for precipitation.

Code	**r**	**DF**	**DF$_{eff}$**	**Proxy**	**Publication**
ak020	0.3	87	33	TRW	ITRDB
ar048	0.28	76	41	TRW	ITRDB
ar049	0.31	81	78	TRW	ITRDB
ar050	0.35	76	58	TRW	ITRDB

Table S2: Proxy records that passed the precipitation screening. Correlation coefficient are calculated with respect to the corresponding grid cell in the CRU TS3 dataset [37] for precipitation.

Code	**r**	**DF**	**DF$_{eff}$**	**Proxy**	**Publication**
ar052	0.35	86	76	TRW	ITRDB
ar053	0.3	81	49	TRW	ITRDB
arge018	0.33	72	32	TRW	ITRDB
arge073	0.32	87	19	TRW	ITRDB
az084	0.39	67	40	TRW	ITRDB
az086	0.41	67	42	TRW	ITRDB
az102	0.49	68	28	TRW	ITRDB
az106	0.48	71	14	TRW	ITRDB
az129	0.29	72	72	TRW	ITRDB
az144	0.42	71	50	TRW	ITRDB
az520	0.33	82	30	TRW	ITRDB
az547	0.3	83	35	TRW	ITRDB
az557	0.31	94	94	TRW	ITRDB
buntgen_science_AMJ_precip	0.23	102	87	TRW	Büntgen et al. 2011, Science
ca051	0.46	66	20	TRW	ITRDB
ca073	0.27	76	35	TRW	ITRDB
ca087	0.5	77	24	TRW	ITRDB
ca528	0.45	83	21	TRW	ITRDB
ca529	0.39	83	25	TRW	ITRDB
ca531	0.43	82	21	TRW	ITRDB
ca532	0.46	83	40	TRW	ITRDB
ca533	0.29	79	46	TRW	ITRDB
ca535	0.28	75	48	TRW	ITRDB
ca612	0.43	89	23	TRW	ITRDB
ca628	0.32	94	19	TRW	ITRDB
ca629	0.3	94	33	TRW	ITRDB
ca632	0.24	95	67	TRW	ITRDB
ca633	0.4	96	35	TRW	ITRDB
cana135	0.42	88	38	TRW	ITRDB
cana136	0.28	88	36	TRW	ITRDB
cana137	0.24	88	37	TRW	ITRDB
cana194	0.32	95	78	TRW	ITRDB

Table S2: Proxy records that passed the precipitation screening. Correlation coefficient are calculated with respect to the corresponding grid cell in the CRU TS3 dataset [37] for precipitation.

Code	**r**	**DF**	**DF$_{eff}$**	**Proxy**	**Publication**
chil002	0.56	68	27	TRW	ITRDB
co066	0.33	74	22	TRW	ITRDB
co067	0.37	74	74	TRW	ITRDB
co076	0.29	66	46	TRW	ITRDB
co509l	0.28	74	71	TRW	ITRDB
co509x	0.27	74	74	TRW	ITRDB
co511	0.27	85	36	TRW	ITRDB
co535	0.38	83	51	TRW	ITRDB
co556	0.27	91	48	TRW	ITRDB
co570	0.38	94	27	TRW	ITRDB
co579	0.34	95	55	TRW	ITRDB
co580	0.32	95	19	TRW	ITRDB
fisher_1996_cgreenland	0.23	78	35	Ice core ^{18}O	Fisher et al. 1996
fl001	0.52	87	47	TRW	ITRDB
ga002	0.31	81	66	TRW	ITRDB
ga003	0.31	81	49	TRW	ITRDB
ga004	0.46	80	80	TRW	ITRDB
helama_sweden_MJ_precip	0.27	89	59	TRW	Helama et al. 2009
id006	0.28	80	74	TRW	ITRDB
id009	0.22	88	64	TRW	ITRDB
id010	0.23	87	71	TRW	ITRDB
il016	0.3	81	39	TRW	ITRDB
jord001	0.28	90	67	TRW	ITRDB
la001	0.3	84	84	TRW	ITRDB
mexi001	0.36	67	43	TRW	ITRDB
mexi022	0.3	88	88	TRW	ITRDB
mexi023	0.28	89	89	TRW	ITRDB
mexi023e	0.25	89	89	TRW	ITRDB
mexi023l	0.29	89	57	TRW	ITRDB
mo037	0.4	88	87	TRW	ITRDB
ms002	0.49	88	63	TRW	ITRDB
nc008	0.37	81	67	TRW	ITRDB

Table S2: Proxy records that passed the precipitation screening. Correlation coefficient are calculated with respect to the corresponding grid cell in the CRU TS3 dataset [37] for precipitation.

Code	**r**	**DF**	**DF$_{eff}$**	**Proxy**	**Publication**
nm025	0.25	68	68	TRW	ITRDB
nm026	0.24	68	36	TRW	ITRDB
nm030	0.42	68	51	TRW	ITRDB
nm031	0.48	68	51	TRW	ITRDB
nm035	0.3	68	20	TRW	ITRDB
nm559	0.44	83	52	TRW	ITRDB
nm560	0.52	85	45	TRW	ITRDB
nm564	0.33	83	26	TRW	ITRDB
nm565	0.25	82	44	TRW	ITRDB
nm572	0.34	88	41	TRW	ITRDB
nv049	0.46	78	37	TRW	ITRDB
nv052	0.29	78	46	TRW	ITRDB
nv053	0.49	78	60	TRW	ITRDB
nv055	0.24	78	74	TRW	ITRDB
nv056	0.35	78	35	TRW	ITRDB
nv058	0.31	78	70	TRW	ITRDB
nv060	0.52	80	30	TRW	ITRDB
nv061	0.42	80	35	TRW	ITRDB
nv507	0.51	72	47	TRW	ITRDB
nv510	0.35	80	26	TRW	ITRDB
nv514	0.31	81	23	TRW	ITRDB
nv515	0.33	76	23	TRW	ITRDB
nv516	0.37	80	31	TRW	ITRDB
nv518	0.48	94	49	TRW	ITRDB
or006	0.44	77	20	TRW	ITRDB
or009	0.49	78	63	TRW	ITRDB
or012	0.37	78	41	TRW	ITRDB
or015	0.34	78	48	TRW	ITRDB
or018	0.43	78	39	TRW	ITRDB
or033	0.33	86	17	TRW	ITRDB
or060	0.35	92	58	TRW	ITRDB
or061	0.37	92	57	TRW	ITRDB

Table S2: Proxy records that passed the precipitation screening. Correlation coefficient are calculated with respect to the corresponding grid cell in the CRU TS3 dataset [37] for precipitation.

Code	**r**	**DF**	**DF$_{eff}$**	**Proxy**	**Publication**
or062	0.36	92	52	TRW	ITRDB
or063	0.44	94	32	TRW	ITRDB
or081	0.3	96	26	TRW	ITRDB
pola006	0.24	81	42	TRW	ITRDB
qian_2003_yriver	0.4	76	76	documentary	Qian et al. 2003
sc004	0.41	81	78	TRW	ITRDB
sd017	0.49	87	55	TRW	ITRDB
spai011	0.23	84	31	TRW	ITRDB
thompson_1992_quelccao18_f	0.31	80	24	Ice core ^{18}O	Thompson et al. 1985
treydte_f	0.26	94	33	Tree ring ^{18}O	Treydte et al. 2006
turk001	0.26	75	23	TRW	ITRDB
tx040	0.47	89	89	TRW	ITRDB
tx042	0.28	88	81	TRW	ITRDB
tx042e	0.27	88	81	TRW	ITRDB
tx042l	0.24	88	88	TRW	ITRDB
ut018	0.28	68	38	TRW	ITRDB
ut022	0.46	67	44	TRW	ITRDB
ut024	0.33	66	28	TRW	ITRDB
ut508	0.35	81	46	TRW	ITRDB
va021	0.28	81	65	TRW	ITRDB
w3crn	0.23	97	44	TRW	ITRDB
w42crn	0.24	97	30	TRW	ITRDB
wimmer_wien_JJA_precip	0.39	92	92	TRW	Wimmer et al. 2000
wy002	0.42	68	11	TRW	ITRDB
wy006	0.45	67	22	TRW	ITRDB
wy019	0.31	86	47	TRW	ITRDB
wy026	0.21	93	25	TRW	ITRDB
r = Correlation coefficient					
DF = Degrees of Freedom					
DF$_{eff}$ = effective DF taking autocorrelation into account					
TRW = Tree Ring Width					
MXD = Maximum Latewood Density					

It is noteworthy that more proxy records passed the correlation screening, but they were not further considered in this study because the statistical results were contradicted by a process-based understanding of the proxy archive i.e., the interpretation in the original publication. The mismatch between statistical outcomes and expert assessment highlights a potential limitation in proxy-selection based only upon correlation analysis. Not in our study, but in general a proxy might also yield equally valid calibration statistics with both temperature and precipitation variation. We have shown (see main text) that temperature and precipitation have distinct variability continuums and thus spectral energy at low frequencies. A proxy simply appears to not be a trustworthy indicator of both variables across all frequencies. The risk is particularly high if a low confidence interval is chosen, if correlations are based on a small number of data points due to temporally low-resolved archives and/or short instrumental records, if significant trends are present, or if long-term dynamical processes such as persistent long-term changes in the North Atlantic Oscillation [38] cause temporal instabilities in the covariance between local temperature and precipitation.

S3 Model simulations

We base the analysis on multi-model ensemble simulations for the last millennium. The models are the ECHO-G model, the COSMOS model, the CCSM3 model, and a 500-year run from the HADCM model. ECHO-G runs (called Erik1 and Erik2) are forced by changes in solar irradiance, greenhouse gases and the radiative effect of volcanic eruptions [39, 40]. For the COSMOS model, the only model which includes an interactive carbon cycle component, an ensemble of five simulations exists (mil0010, mil0012, mil0021, mil0025, mil0026; [41]). It additionally to ECHO-G includes aerosol forcing and land-use changes. Solar irradiance of three ensemble members has a reduced amplitude compared to the ECHO-G simulations due a new reconstruction and on-going debate about the true amplitude. The HADCM [42] and the CCSM3 simulations [43] are forced like the ECHO-G simulations, but they use updated and additional forcings for total solar irradiance, greenhouse gases, volcanic aerosols, and land-use changes.

S4 Model simulation β-value maps

In the main article we present the β-value maps of the model simulation as an average. In Fig. S2 and S3, the β-value maps for each single simulation highlight that the models simulate comparable variability continua, which justifies the construction of a model average.

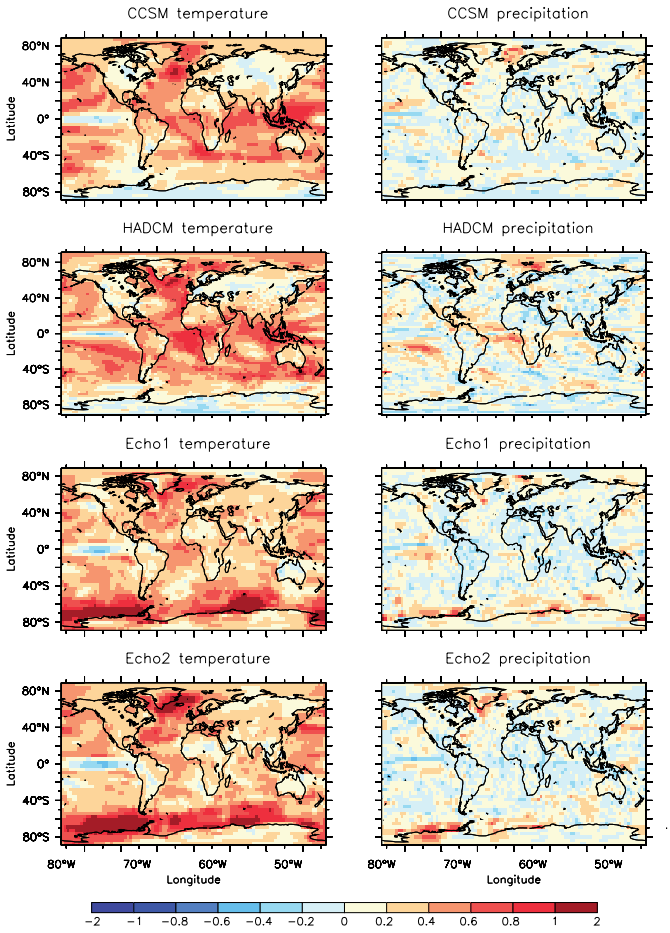

Figure S2: β-value maps of single model simulations - part 1.

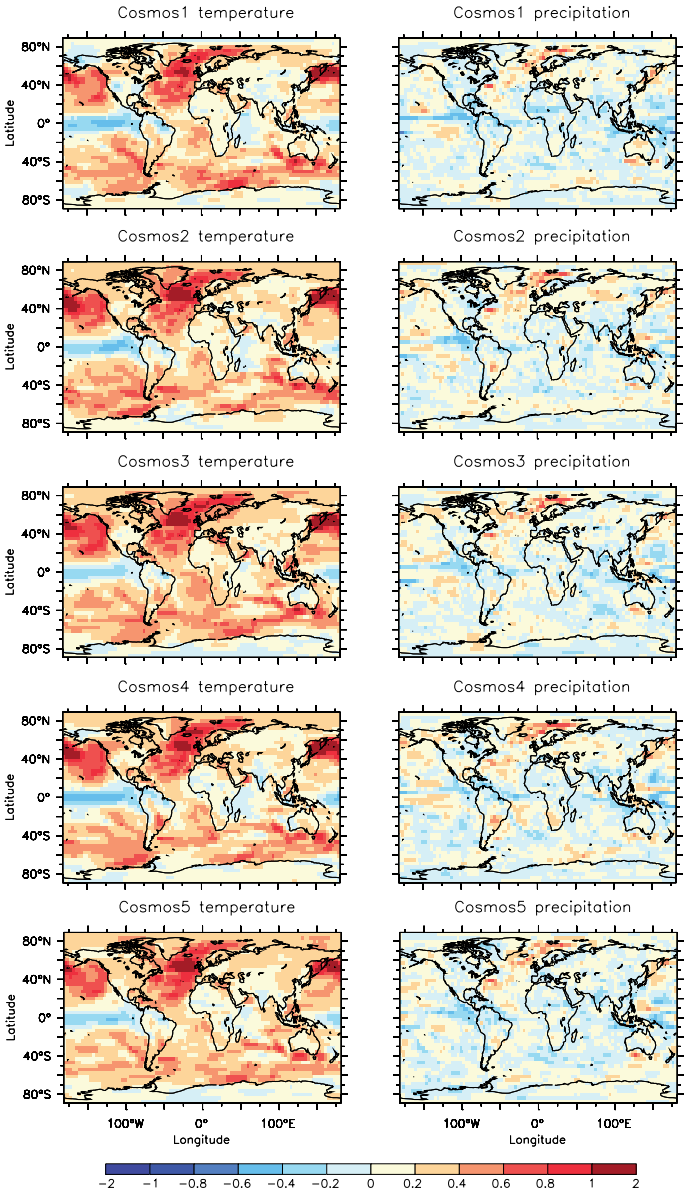

Figure S3: β-value maps of single model simulations - part 2.

S5 β-value sensitivity to spatial grid resolution

The spatial resolution might influence spectral characteristics especially for variables with high spatial variability such as precipitation because the coarser the grid, the more records are averaged. The β-values for the instrumental CRU TS3 dataset at resolutions of 0.5 to 2.5 degrees result in nearly identical β estimates and thus suggest no significant influence of spatial averages over grid boxes (Fig. S4).

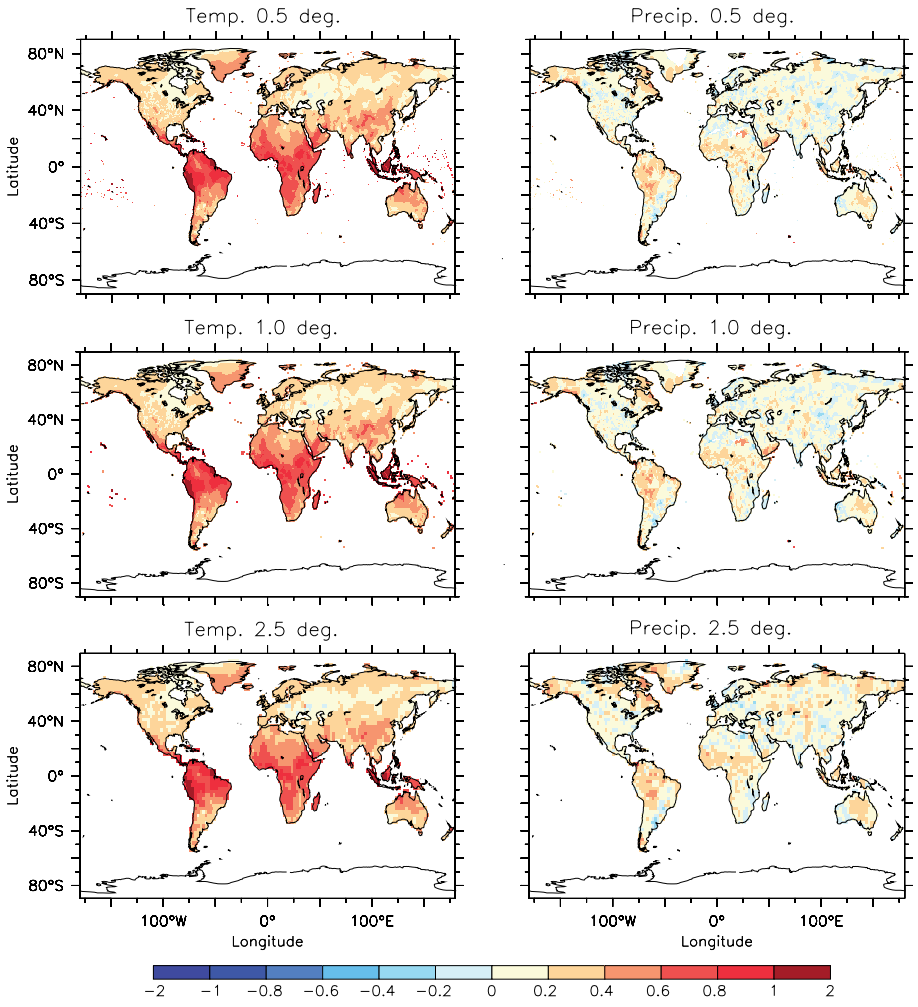

Figure S4: CRU TS3 temperature and precipitation β-value maps for various spatial resolutions (grid of 0.5, 1.0 and 2.5 degrees in longitudinal and latitudinal direction).

S6 Seasonality and time-scale dependency of β estimates

Seasonal differences in the β-value patterns are small (Fig. S5). In an analysis of the CCSM model temperature for the months December to February and June to August, we find slightly higher β-values over continental northern Asia and in North America during northern hemisphere summer (JJA). However, all main features such as the land-sea contrast and decreasing β-values toward high latitudes

are robust and indicate no significant seasonal dependence.

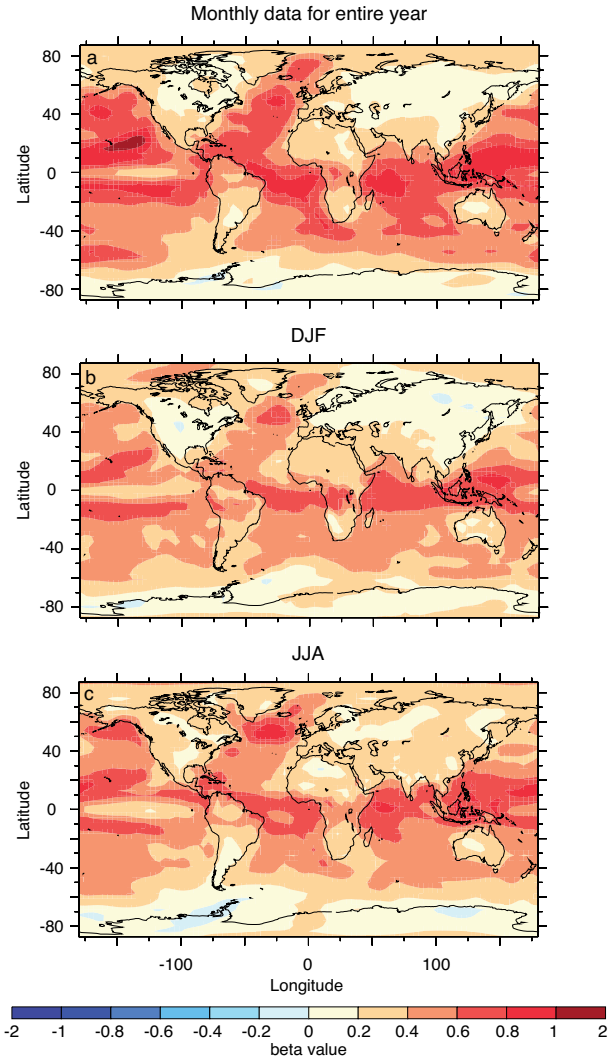

Figure S5: CCSM temperature β-value maps based on a) monthly data of the entire year, b) monthly data of the months December to February and c) the same for June to August.

The length and resolution of the proxy data challenges the analysis of a common frequency range. In Fig. S6 to S9 we investigate gridded instrumental data and a model simulation, to see the consequences of the selected frequency range. Moving from 2 months to 20 years (left to right column) as a high frequency cut-off, the number of data points in the spectral domain to fit a least-squares functions drops dramatically. Consequently, the results become more uncertain/noisy, as indicated by extremely contradictory positive and negative β values in neighboring grid boxes.

The low-frequency end of the spectrum has less implications because much longer records are required to increase the number of data points for low-frequency variability. For best comparability between the various datasets and due to an observed break in the otherwise time-scale independent β at frequencies of 1/(100 years) [44], we set the low-frequency limit at 100 years.

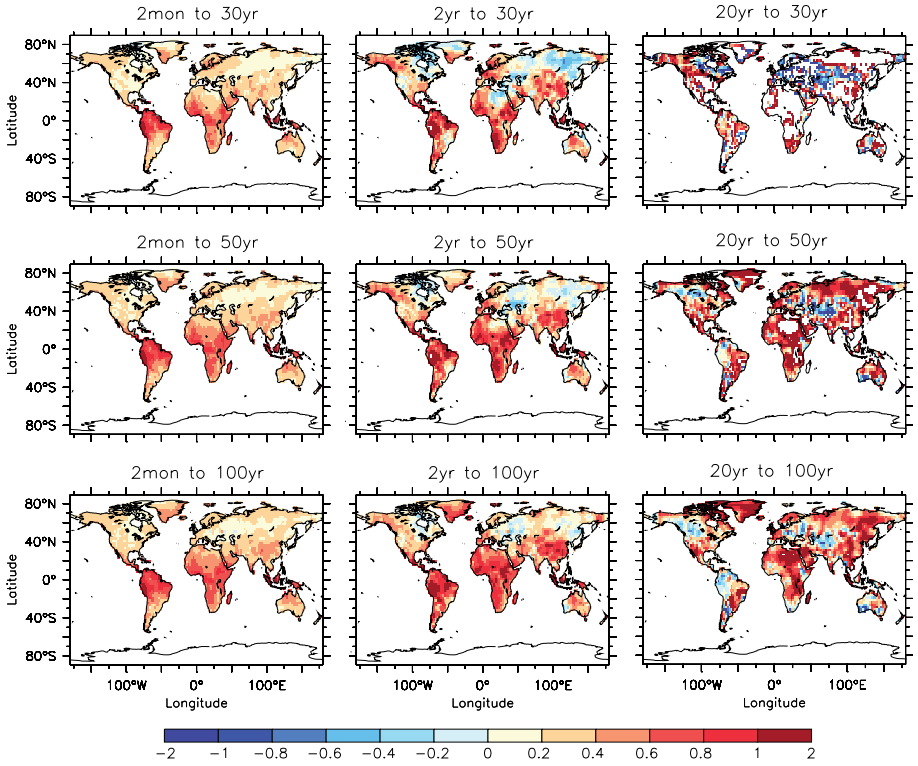

Figure S6: CRU TS3 temperature β-value maps for various frequency ranges.

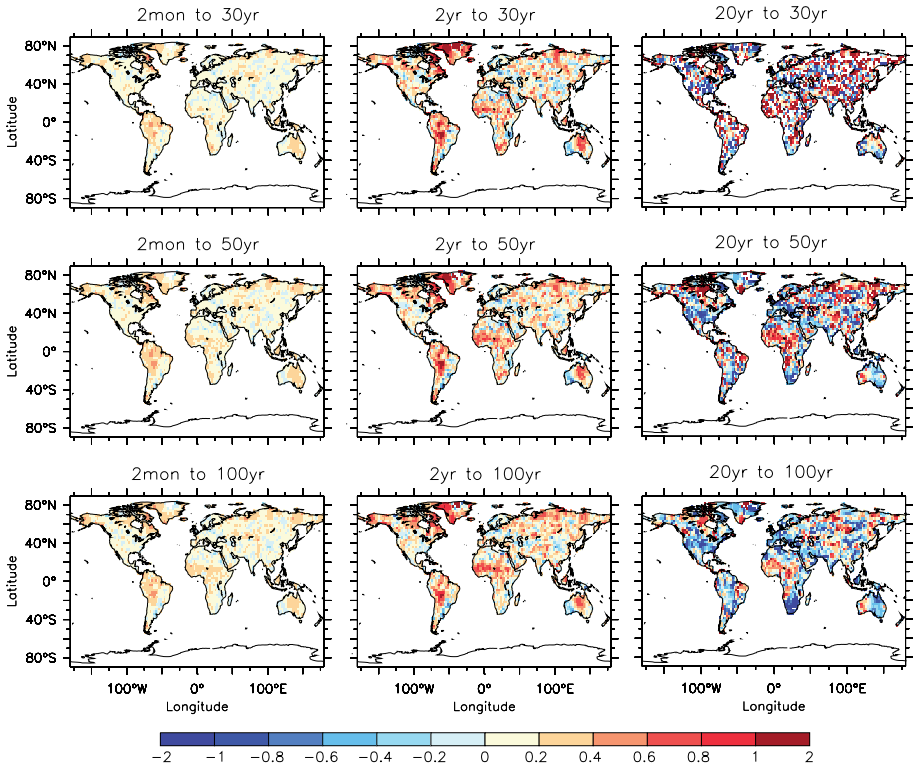

Figure S7: CRU TS3 precipitation β-value maps for various frequency ranges.

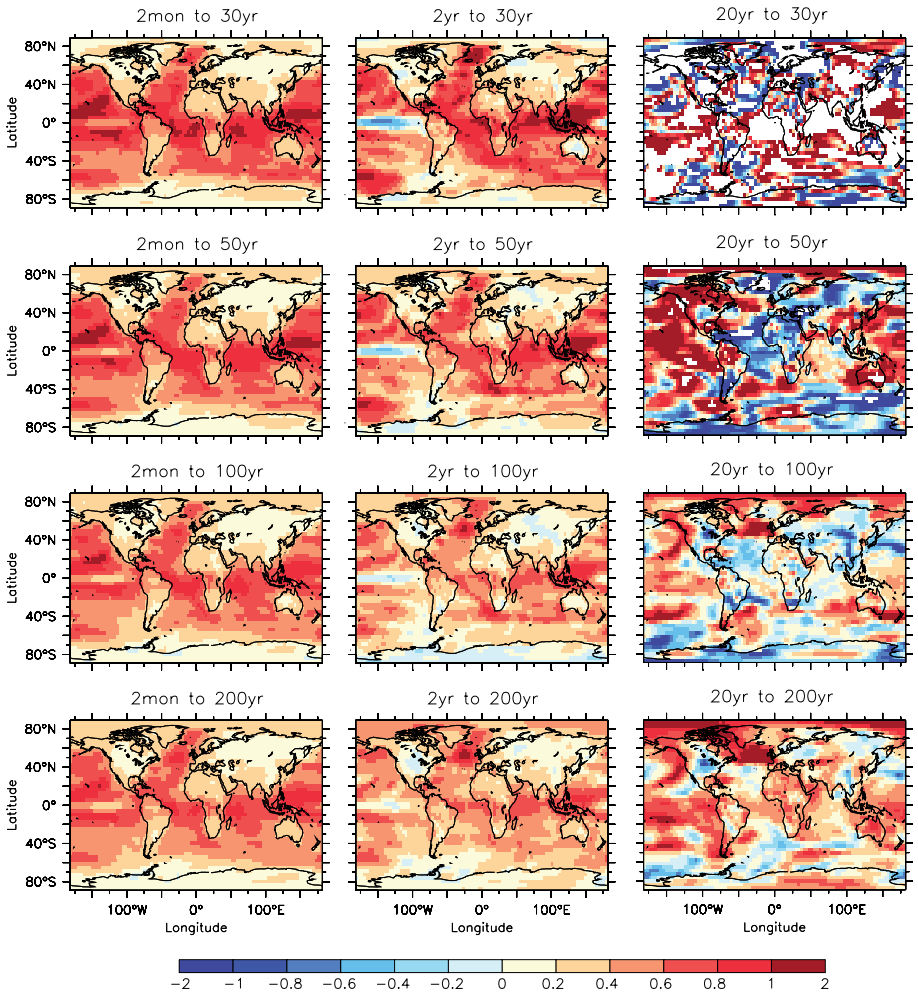

Figure S8: CCSM temperature β-value maps for various frequency ranges.

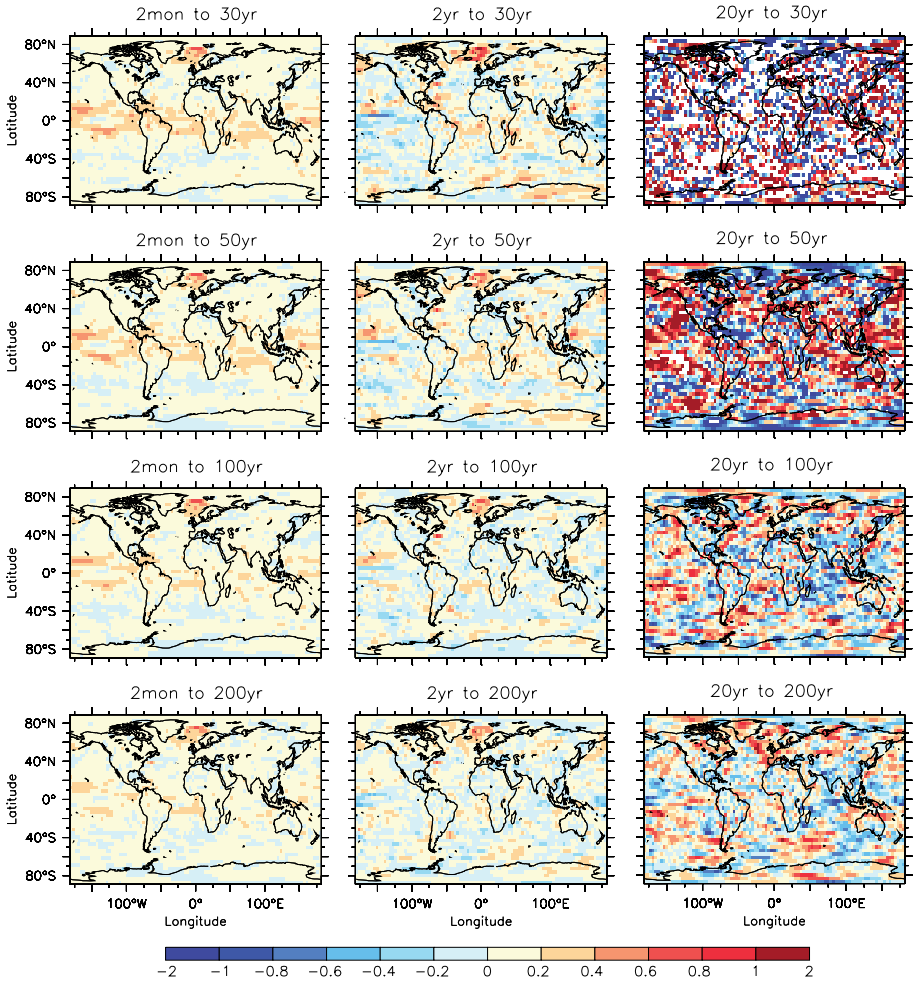

Figure S9: CCSM precipitation β-value maps for various frequency ranges.

S7 Early instrumental, proxy and model β-value maps

Instrumental temperature and precipitation records with a length of more than 200 years are primarily found in Europe. β-values of these series for the 1/(2 years) to 1/(100 years) frequency range confirm that temperature series are redder than precipitation records (Fig. S10a and b) as seen in shorter series of the CRU TS3 data set.

This difference cannot be observed in proxy data (Fig. S10c and d). Neither can relationships between the proxy spectral characteristics and their locations be found ((Fig. S10c and d). Furthermore, spatially proximal proxies often differ substantially in their β-values even if the proxy type is identical (e.g. in the case of tree-ring width in the western United States).

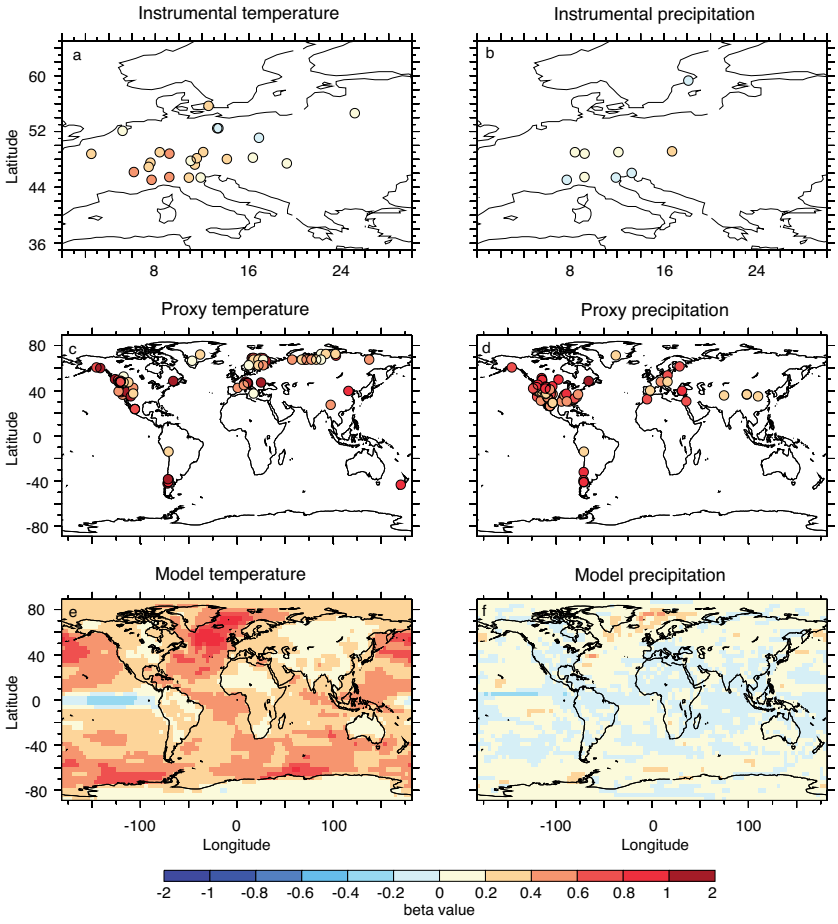

Figure S10: β-value maps early instrumental measurements for a) temperature and b) precipitation, the same for proxies that pass the screening for c) temperature and d) precipitation sensitivity. Model results are presented for comparison in e) and f). All β-value are calculated for the frequencies range between 1/(2 years) and 1/(100 years).

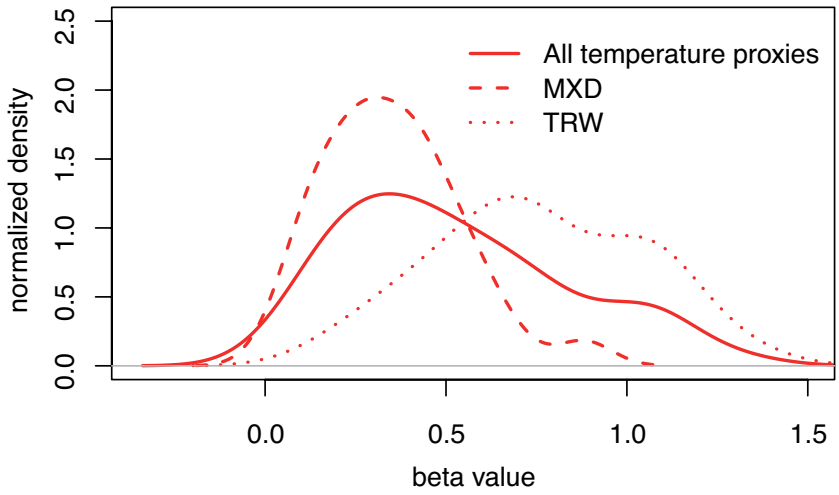

Figure S11: β-value distribution of all temperature proxies (solid line), for a subset of 29 MXD proxies (dashed) and 25 TRW records (dotted).

S8 β-value distributions for individual proxy types

Collectively, we found the proxy datasets for both temperature and precipitation to be biased red with beta values for the individual proxy records ranging from 0.04 to 1.31 — a rather wide spread. For the two most commonly used proxy types in temperature reconstruction of the past millennium, TRW and MXD, there were enough records to evaluate if the proxy type is related to the beta-value distribution. In these distributions we find a strong red biases for TRW in comparison with instrumental data (Fig. S11). MXD, in contrast, is on average only slightly biased. Especially in TRW there is also more variability in beta-values than expected by instrumental data or climate models demonstrating the significance of spectral noise in these data.

S9 Mixed temperature and precipitation signals

Proxy records can contain mixed signals of temperature and hydroclimatic conditions and can correlate with both temperature and precipitation. There are two reasons: first, both variables influence the proxy, as in the case of tree growth and second, climatic variables are seasonally and/or spatially correlated (see next section). In the frequency domain, adding a time series with a white spectrum to another series with a red spectrum will usually lead to an intermediate, slightly red spectrum [45]. This is at least the case if the time series are uncorrelated. Theoretically, we could think of a special case - as mentioned in the main article - where temperature and precipitation variability correlate at low frequencies and anti-correlate at high frequencies, reducing their variability at high frequencies. This would lead to increased

redness due to a mixed signal. A real world example is the Palmer Drought Severity Index (PDSI, [46]) which is a measure of soil moisture availability and is mainly influenced by temperature and precipitation. β-value distributions of instrumental temperature, precipitation and instrumental data-based PDSI for the United States show the expected pattern of nearly white precipitation, red temperature spectra and PDSI lying in between (Fig. S12). A proxy-based PDSI reconstruction[47] for the same region highlights again a slight red bias, likely stemming from the input proxy data even though these reconstructions were explicitly developed to have the same autoregressive properties as the instrumental PDSI.

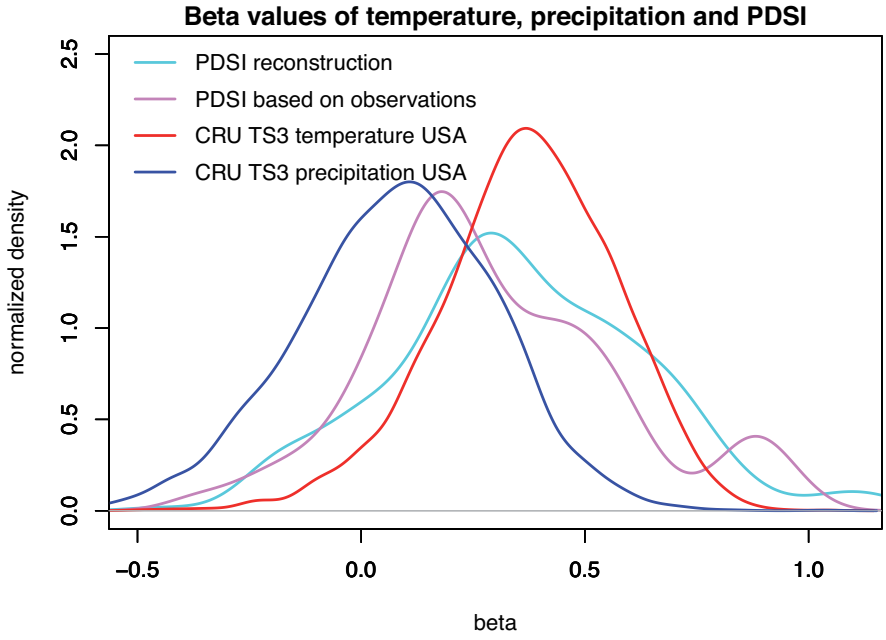

Figure S12: β-value distribution for instrumental temperature and precipitation over the continental United States of America without Alaska. The same for the PDSI calculated based on instrumental data and proxy data.

S10 Spectral color of multi-proxy climate field reconstructions

In addition to Fig. 3 (main paper) we investigate the spectral color of the only global multi-proxy, climate-field reconstructions for the last millennium [48]. Here we focus on periods between 20 and 200 years because "only interdecadal and longer-term variations are meaningfully resolved" in this reconstruction. The results suggest significant red biases (Fig. S13) in comparison to the model simulations. While not excluding possibilities for white biases in models [49], the exceptionally red spectra for nearly the entire spatial domain of the Mann et al. (2009) reconstruction, is consistent both with the overestimation of low frequency variability in the proxy records and the results seen for the South American reconstructions (Fig. 3).

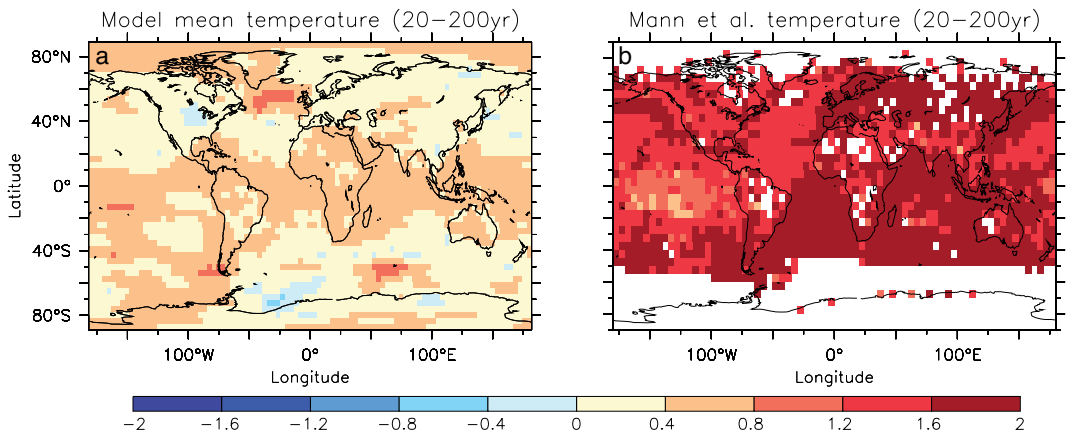

Figure S13: a) Mean spectral color of the model ensemble and b) the decadally resolved climate-field reconstructions [48]; both for periods between 20 years and 200 years.

S11 Correlation between temperature and precipitation

Most [50, 48], but not all [51], state of the art climate reconstruction methods use the covariance structure and thus include precipitation records in temperature reconstructions because temperature and precipitation are regionally and seasonally correlated (Fig. S14). Temperature and precipitation are for instance positively correlated in European winter (Fig. S14b) and negatively correlated in European summer (Fig. S14c). This could lead to an incorrect selection of winter precipitation proxies for European temperature reconstructions. This is especially a risk, because sparse data causes seasonal records to be used in annual mean reconstructions.

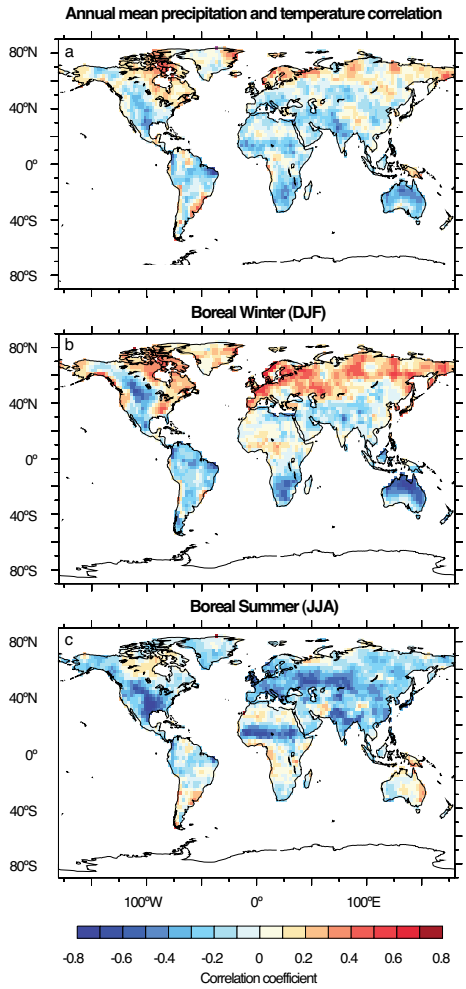

Figure S14: Correlation between temperature and precipitation: (a) annual mean, (b) boreal winter and (c) boreal summer. The correlation patterns are based on the gridded CRU TS3 data [37].

Acknowledgements

This study was funded by the EU project MILLENNIUM (#017008-GOCE) and by the Swiss National Science Foundation (SNSF) through its National Center of Competence in Research on Climate (NCCR Climate). C. Raible und S. Brönnimann are also supported by the Synergia project FUPSOL, C. Raible additionally by the EU project Past4Future. We thank everyone who contributed model or proxy data for this study. Support for the Twentieth Century Reanalysis Project dataset is provided by the U.S. Department of Energy, Office of Science Innovative and Novel Computational Impact on Theory and Experiment (DOE INCITE) program, and Office of Biological and Environmental Research (BER), and by the National Oceanic and Atmospheric Administration Climate Program Office. We thank Erin Gleeson for her editing efforts.

References

[1] Büntgen, U., Frank, D., Nievergelt, D. & Esper, J. Summer temperature variations in the European Alps, AD 755–2004. *Journal of Climate* **19**, 5606–5623 (2006).

[2] Qian, W., Hu, Q., Zhu, Y. & Lee, D.-K. Centennial-scale dry-wet variations in East Asia. *Climate Dynamics* **21**, 77–89 (2003).

[3] Cronin, T., Dwyer, G., Kamiya, T. & Schwede, S. Medieval Warm Period, Little Ice Age and 20^{th} century temperature variability from Chesapeake Bay. *Global and Planetary Change* **36**, 17–29 (2003).

[4] Tiljander, M., Saarnisto, M., Ojala, A. & Saarinen, T. A 3000-year palaeoenvironmental record from annually laminated sediment of Lake Korttajärvi, Central Finland. *Boreas* **32**, 566–577 (2003).

[5] Verschuren, D., Laird, K. R. & Cumming, B. F. Rainfall and drought in equatorial east Africa during the past 1,100 years. *Nature* **403**, 410–414 (2000).

[6] Ge, Q., Zheng, J., Fang, X., Man, Z. & Zhang, X. Winter half-year temperature reconstruction for the middle and lower reaches of the Yellow River and Yangtze River, China, during the past 2000 years. *The Holocene* **13**, 933–940 (2003).

[7] Mann, M. *et al.* Proxy-based reconstructions of hemispheric and global surface temperature variations over the past two millennia. *Proceedings of the National Academy of Sciences* **105**, 13252–13257 (2008).

[8] Kirchhefer, A. (2012). Personal communication.

[9] Grudd, H. Torneträsk tree-ring width and density AD 500-2004: a test of climatic sensitivity and a new 1500-year reconstruction of North Fennoscandian summers. *Climate Dynamics* **31**, 843–857 (2008).

[10] Gunnarson, B. E., Linderholm, H. W. & Moberg, A. Improving a tree-ring reconstruction from west-central Scandinavia: 900 years of warm-season temperatures. *Climate Dynamics* **36**, 97–108 (2011).

[11] Helama, S., Merilainen, J. & Tuomenvirta, H. Multicentennial megadrought in northern Europe coincided with a global El Nino-Southern Oscillation drought pattern during the Medieval Climate Anomaly. *Geology* **37**, 175–178 (2009).

[12] Helama, S. *et al.* Dendroclimatic transfer functions revisited: Little Ice Age and Medieval Warm Period summer temperatures reconstructed using artificial neural networks and linear algorithms. *Annales Geophysicae* **27**, 1097 (2009).

[13] Büntgen, U. *et al.* 2500 years of European climate variability and human susceptibility. *Science* **331**, 578–582 (2011).

[14] Büntgen, U., Frank, D., Neuenschwander, T. & Esper, J. Fading temperature sensitivity of Alpine tree growth at its Mediterranean margin and associated effects on large-scale climate reconstructions. *Climatic Change* (2012).

[15] Büntgen, U., Frank, D., Carrer, M., Urbinati, C. & Esper, J. Improving alpine summer temperature reconstructions by increasing sample size. *TRACE* **7**, 36–43 (2009).

[16] Büntgen, U., Esper, J., Frank, D. C., Nicolussi, K. & Schmidhalter, M. A 1052-year tree-ring proxy for alpine summer temperatures. *Climate Dynamics* **25**, 141–153 (2005).

[17] Corona, C. *et al.* Millennium-long summer temperature variations in the European Alps as reconstructed from tree rings. *Climate of the Past* **6**, 379–400 (2010).

[18] Wimmer, R., Strumia, G. & Holawe, F. Use of false rings in Austrian pine to reconstruct early growing season precipitation. *Canadian Journal of Forest Research* **30**, 1691–1697 (2000).

[19] Esper, J., Büntgen, U., Frank, D. C., Pichler, T. & Nicolussi, K. Updating the Tyrol tree-ring dataset. In K. Haneca et al. (ed.) *Tree rings in archaeology, climatology and ecology*, 80–85 (TRACE, 2007).

[20] Carrer, M., Nola, P., Eduard, J. L., Motta, R. & Urbinati, C. Regional variability of climate-growth relationships in Pinus cembra high elevation forests in the Alps. *Journal of Ecology* **95**, 1072–1083 (2007).

[21] Büntgen, U., Frank, D., Grudd, H. & Esper, J. Long-term summer temperature variations in the Pyrenees. *Climate Dynamics* **31**, 615–631 (2008).

[22] Popa, I. & Kern, Z. Long-term summer temperature reconstruction inferred from tree-ring records from the Eastern Carpathians. *Climate Dynamics* **32**, 1107–1117 (2009).

[23] Esper, J. *et al.* Long-term drought severity variations in Morocco. *Geophysical Research Letters* **34**, L17702 (2007).

[24] Esper, J., Cook, E. & Schweingruber, F. Low-frequency signals in long tree-ring chronologies for reconstructing past temperature variability. *Science* **295**, 2250–2253 (2002).

[25] Esper, J., Frank, D. C., Wilson, R. J. S., Büntgen, U. & Treydte, K. Uniform growth trends among Central Asian low-and high-elevation juniper tree sites. *Trees-Structure and Function* **21**, 141–150 (2007).

[26] Treydte, K. S. *et al.* The twentieth century was the wettest period in northern Pakistan over the past millennium. *Nature* **440**, 1179–1182 (2006).

[27] Esper, J. *et al.* Temperature-sensitive tien shan tree ring chronologies show multi-centennial growth trends. *Climate Dynamics* **21**, 699–706 (2003).

[28] Yang, B., Braeuning, A., Johnson, K. & Shi, Y. General characteristics of temperature variation in China during the last two millennia. *Geophysical Research Letters* **29**, 1324 (2002).

[29] Zhang, Q., Cheng, G., Yao, T., Kang, X. & Huang, J. A 2,326-year tree-ring record of climate variability on the northeastern Qinghai-Tibetan Plateau. *Geophysical Research Letters* **30**, 1739 (2003).

[30] Hantemirov, R. & Shiyatov, S. A continuous multimillennial ring-width chronology in Yamal, northwestern Siberia. *Holocene* **12**, 717–726 (2002).

[31] Loso, M. G. Summer temperatures during the Medieval Warm Period and Little Ice Age inferred from varved proglacial lake sediments in southern Alaska. *Journal of Paleolimnology* **41**, 117–128 (2009).

[32] Bird, B. W., Abbott, M. B., Finney, B. P. & Kutchko, B. A 2000 year varve-based climate record from the central Brooks Range, Alaska. *Journal of Paleolimnology* **41**, 25–41 (2009).

[33] McKay, N. P. & Kaufman, D. S. Holocene climate and glacier variability at Hallet and Greyling Lakes, Chugach Mountains, south-central Alaska. *Journal of Paleolimnology* **41**, 143–159 (2009).

[34] Luckman, B. H. & Wilson, R. J. S. Summer temperatures in the Canadian Rockies during the last millennium: a revised record. *Climate Dynamics* **24**, 131–144 (2005).

[35] Thomas, E. K. & Briner, J. P. Climate of the past millennium inferred from varved proglacial lake sediments on northeast Baffin Island, Arctic Canada. *Journal of Paleolimnology* **41**, 209–224 (2009).

[36] Salzer, M. W. & Kipfmueller, K. F. Reconstructed temperature and precipitation on a millennial timescale from tree-rings in the Southern Colorado Plateau, U.S.A. *Climatic Change* **70**, 465–487 (2005).

[37] Mitchell, T. D. & Jones, P. D. An improved method of constructing a database of monthly climate observations and associated high-resolution grids. *International Journal of Climatology* **25**, 693–712 (2005).

[38] Trouet, V. *et al.* Persistent positive North Atlantic Oscillation mode dominated the Medieval Climate Anomaly. *Science* **324**, 78–80 (2009).

[39] González-Rouco, J. F., Beltrami, H., Zorita, E. & von Storch, H. Simulation and inversion of borehole temperature profiles in surrogate climates: spatial distribution and surface coupling. *Geophysical Research Letters* **33**, L01703 (2006).

[40] Zorita, E., González-Rouco, F. & von Storch, H. Comments on "testing the fidelity of methods used in proxy-based reconstructions of past climate". *Journal of Climate* **20**, 3693–3698 (2007).

[41] Jungclaus, J. H. *et al.* Climate and carbon-cycle variability over the last millennium. *Climate of the Past* **6**, 723–737 (2010).

[42] Tett, S. *et al.* The impact of natural and anthropogenic forcings on climate and hydrology since 1550. *Climate Dynamics* **28**, 3–34 (2007).

[43] Hofer, D., Raible, C. C. & Stocker, T. F. Variations of the Atlantic meridional overturning circulation in control and transient simulations of the last millennium. *Climate of the Past* **7**, 133–150 (2011).

[44] Huybers, P. & Curry, W. Links between annual, Milankovitch and continuum temperature variability. *Nature* **441**, 329–332 (2006).

[45] Osborn, T. & Briffa, K. Climate: The real color of climate change? *Science* **306**, 621–622 (2004).

[46] Palmer, W. Meteorological drought. Tech. Rep., U.S. Department of Commerce, Weather Bureau (1965). Research Paper No. 65.

[47] Cook, E., Woodhouse, C. & Eakin, C. Long-term aridity changes in the western United States. *Science* **306**, 1015–1018 (2004).

[48] Mann, M. E. *et al.* Global signatures and dynamical origins of the Little Ice Age and Medieval Climate Anomaly. *Science* **326**, 1256–1260 (2009).

[49] DelSole, T. Low-frequency variations of surface temperature in observations and simulations. *Journal of Climate* **19**, 4487–4507 (2006).

[50] Jones, P. *et al.* High-resolution palaeoclimatology of the last millennium: a review of current status and future prospects. *The Holocene* **19**, 3–49 (2009).

[51] Franke, J., González-Rouco, J. F., Frank, D. & Graham, N. E. 200 years of European temperature variability: insights from and tests of the Proxy Surrogate Reconstruction Analog Method. *Climate Dynamics* **37**, 133–150 (2011).